

Application of Local Radon Transforms for dip-dependent GPR image decomposition

Ulrich Theune*, Mauricio D. Sacchi, and Douglas R. Schmitt, Department of Physics, University of Alberta

Summary

GPR is a powerful tool for geophysical near-surface investigations. It is capable of delivering a high-resolution image of the subsurface structure. However, if the underground consists of many reflecting events, the analysis and interpretation of the data can be very complicated. In this paper, we report on a new image decomposition technique that is based on Local Radon transforms. This technique is a parametric local dip-decomposition method that allows us to extract features or reconstruct GPR data. After reconstructing the data with only a subset of dips, the interpretation of the data improves substantially. We demonstrate the capabilities of this technique at GPR data acquired at the highly fractured summit of Turtle Mountain (Alberta/Canada).

Introduction

Ground penetrating radar (GPR) has become a frequently employed technique in geophysical near surface investigation. GPR data are an image of the dielectric structure of the subsurface with high vertical and horizontal resolution. It has therefore gained popularity for near-surface studies in many civil engineering and environmental applications (e.g., Zeng and McMechan, 1997) as well as archaeological studies (e.g., Goodman et al., 1995), among others. However, the analysis of GPR images can be complicated in highly structured media, where numerous events may overlap, and hamper the interpretation. An example for that are the GPR data that were acquired at Turtle Mountain in Alberta, Canada, to map bedding planes and fractures for a slope stability estimation project (Theune et al., 2005). The unmigrated data are shown in Fig. 1.

The highly fractured nature of the rock is apparent in the GPR image through many reflectors of various dips. There are several reflectors that dip "downwards" with increasing distance along the profile. Examples of this reflector pattern are indicated by black arrows in Fig. 1. A second set of reflectors, less in number and reflected amplitude strength, is present between 0 and 40 m profile length with "upward" dips along the survey line (green arrows). However, numerous other events complicate the analysis of the image. The situation becomes worse after migration (Fig. 3a).

Different techniques have been applied to improve the image of quality: Cagnoli and Ulrych (2001) applied singular value decomposition, and Nuzzo and Quarta (2004) used wavelet and $\tau-p$ (or linear Radon) transforms, to mention a few. The chief problem of many techniques is that they operate globally on the entire data set, thus they may not represent local features very well. For example, the per-

formance of Radon transforms breaks down if there is a mismatch between the transform's integration path and the traveltime signature in the data.

In this paper, we explore the potential of Local Radon transforms to achieve dip-dependent image decomposition of GPR data. Radon transforms have a long history in seismic data processing to remove coherent noise such as ground roll or multiples (Ulrych et al., 1999). In addition, Radon transforms are also often used in image analysis for feature extraction. Here, we employ the combination of the concepts of generalized convolution and Local Radon transforms, as described by Sacchi et al. (2004), to enhance and extract features in GPR images.

Methodology

Radon transforms can be interpreted as a "search for coherent events" in seismic or GPR data sets. In a typical seismic application, data amplitudes are summed along certain integration paths, which are usually either linear, parabolic, or hyperbolic and extend over the entire offset of the data. For example, a linear coherent event such as ground roll will have a large summation value for a particular search direction.

The principal idea of Local Radon transforms is to use a short summation path that is applied locally at each $x-t$ -point in the data set. In our application, we employ a linear Local Radon operator of the form that is given in the Fourier domain by (Sacchi et al., 2004)

$$\hat{b}(x, \omega, p) = \hat{s}(\omega)h(x)e^{i\omega p \cdot x}, \quad -\ell_0 \leq x \leq \ell_0. \quad (1)$$

In this expression, $\hat{s}(\omega)$ is ideally the real wavelet; in reality, the wavelet is often unknown. Therefore, we choose an approximation to the wavelet instead. The variable $h(x)$ is a spatial taper that gives larger weights to the center of the operator, and $p \cdot x$ is the linear integration path with dip p . ℓ_0 defines the operator half-width. After applying Fourier transform, we obtain the operator in the data domain,

$$b(x, t, p) = \mathcal{F}^{-1}[\hat{b}(x, \omega, p)]. \quad (2)$$

This operator is now applied at every point (x_0, t_0) of the data set. In doing so, we obtain a measure for the local data coherence at each data point for the operator $b(x - x_0, t - t_0, p)$. We denote this measure by $f_p(x_0, t_0)$. Applying this operation to the entire data results into a new set of data $d_p(x, t)$ that we call the p -mode:

$$d_p(x, t) = \sum_{x_0} \sum_{t_0} f_p(x_0, t_0) b(x - x_0, t - t_0, p). \quad (3)$$

Dip-dependent GPR image decomposition

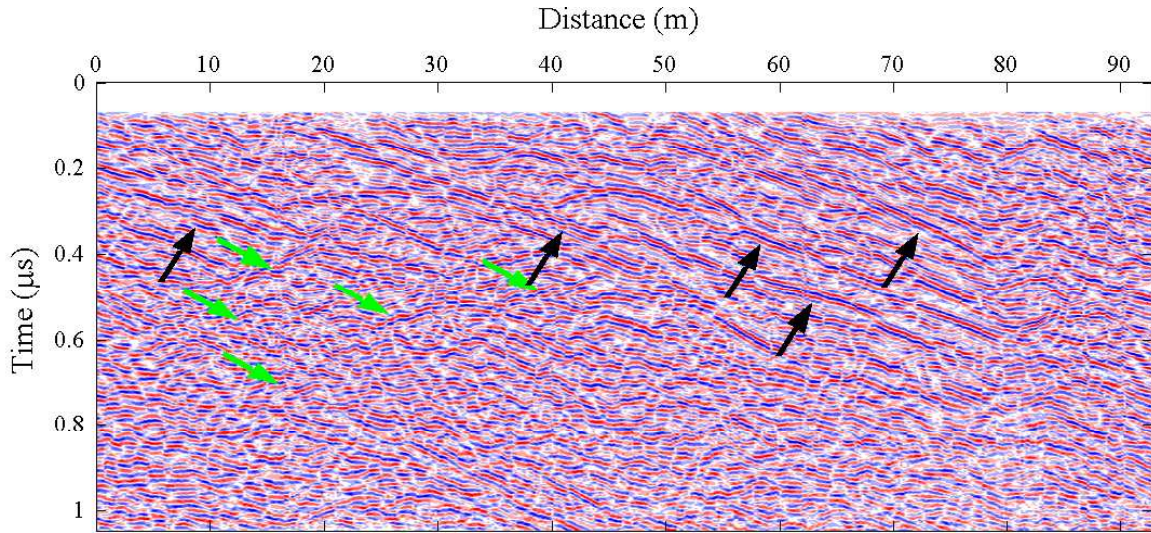


Fig. 1: Unmigrated GPR data acquired at Turtle Mountain.

This last equation can also be written in matrix form as $\mathbf{D}_p = \mathbf{F}_p \otimes \mathbf{B}(p)$. The last expression is referred to as *generalized convolution*. Sacchi et al. (2004) interpreted the parameter \mathbf{F}_p as shaping filters that transform the operators $\mathbf{B}(p)$ into the data \mathbf{D}_p . These filter panels are determined from the data by minimizing the following cost function \mathcal{J} ,

$$\mathcal{J} = \|\mathbf{D} - \sum_{p=1}^{N_p} \mathbf{F}_p \otimes \mathbf{B}(p)\|_2^2. \quad (4)$$

Determining \mathbf{F}_p from the data is analogous to finding the deconvolution operator. Hence, we may call this operation *generalized deconvolution*. The cost function \mathcal{J} is minimized using the method of conjugate gradients. The inner products in the algorithm are efficiently implemented in the Fourier domain with FFTs.

After determining the filters \mathbf{F}_p , we can construct a synthetic image of the data using all dips p , $\bar{\mathbf{D}}$, by generalized convolution. Another possibility is to synthesize a data set $\bar{\mathbf{D}}$ using only a subset S_p of the available dips,

$$\bar{\mathbf{D}}(x, t) = \sum_{p \in S_p} \mathbf{F}_p(x, t) \otimes \mathbf{B}(x, t, p) \quad (5)$$

Such an operation may be called *generalized filtering*. The selection of the subset of modes can be chosen such that linear events of a particular dip are removed or retained. Removing linear events such as ground roll would be a typical application in seismic data processing. In the example introduced in the following section, we synthesized several data sets $\bar{\mathbf{D}}$ with narrow dip ranges to isolate reflectors in the data.

A workflow for dip-dependent image decomposition may look like:

1. We start with data after initial processing consisting of topographic corrections, amplitude gain, and bandpass filtering.
2. Then, we migrate the data using a constant velocity Kirchhoff migration algorithm. The resulting image will be used to test the data reconstruction.
3. Using *generalized deconvolution*, we decompose the image into N_p modes with different dips.
4. Now, we reconstruct the data using *generalized convolution*. This data set should be close to the original data.
5. Alternatively, we can use only a subset of the available data modes to extract certain dips in the data (i.e., *generalized filtering*). We can then migrate the new data set to visualize the chosen dips and compare them with the original data.

The chart in Fig. 2 shows this workflow symbolically.

Example

We applied generalized deconvolution to a GPR data set that was acquired at the highly fractured summit of Turtle Mountain in Alberta, Canada. The main purpose of these measurements was to detect fractures and to map bedding planes for geotechnical slope stability studies. There are two dominating reflector patterns in the data that we have indicated by black and green arrows, respectively. However, due to the presence of dense fracture systems that often overlap, the interpretation of the migrated data is complicated.

To improve the image analysis, we decomposed the data into 25 modes, where the dip p varied between

Dip-dependent GPR image decomposition

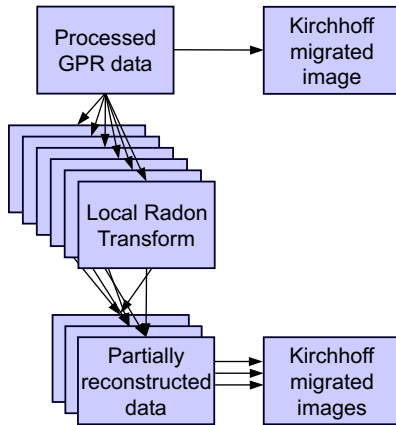


Fig. 2: Flow diagram for generalized deconvolution and filtering.

-60.0 ns/m and 60.0 ns/m . Since the wavelet of the propagating electro-magnetic wave is unknown, we approximated it by a Ricker wavelet with a central frequency of 50 MHz. Furthermore, we chose the aperture half-width (ℓ_0) to be 1 m, which is equivalent to including 10 GPR traces into the local operator. Finally, a Hamming window was used as the taper function $h(x)$.

We then synthesized data sets using only narrow ranges of dips that represent a reflector pattern in the data and subsequently applied Kirchhoff migration. For the data shown in Fig. 3b, we used only dips in the range $0.005 \text{ ns/m} \leq p \leq +0.019 \text{ ns/m}$, and only dips with $-0.015 \text{ ns/m} \leq p \leq 0.00 \text{ ns/m}$ were considered in the data synthesis shown in Fig. 3c. When comparing these images with the migration results of the original data (Fig. 3a), it is apparent that the interpretation of the data is less ambiguous in the synthesized data. This is especially evident in the details shown in Fig. 4. Fig. 4a is a detail of the original data set after migration. For this part of the data, it is very difficult to infer any features from the data that may indicate coherent reflectors. This is contrasted by the details shown in Fig. 4b and c that clearly show coherent events in this section of the data (Fig. 4b shows a detail from the migrated image in Fig. 3b, Fig. 4c is taken from Fig. 3c).

Conclusions

The concept of generalized convolution applied to Local Radon transforms for dip dependent image decomposition allows for the extraction of desired features in GPR data, in our case reflectors with a particular dip. After partial image reconstruction using only a subset of the available data modes \mathbf{D}_p , coherent events, previously superimposed by numerous reflectors with different dips, are much easier to detect. The interpretation of the data therefore improves significantly. We applied this method to extract and enhance coherent features in the data. However, other applications to remove coherent features are possible as well. Examples are removal of "system ringing" or strong off-side reflections from metal

constructions near a GPR survey area.

Acknowledgments

We like to thank David Cruden, Mike deGroot, Julia Holzhauser, Dan Kenway, Dean Rokosh, Marek Welz, and Willem Langenberg for their assistance in acquiring and interpreting the GPR data. The data acquisition and analysis was funded by NSERC, the Canada Research Chair program, both granted to D.R. Schmitt, and the SAIG consortium at the University of Alberta.

References

- Cagnoli, B., and T.J. Ulrych, Singular value decomposition and wavy reflections in ground-penetrating radar images of base surge deposits, *Journal of Applied Geophysics*, Vol.48, 175-182, 2001.
- Goodman, D., Y. Nishimura, and J. Rogers, GPR time slices in archaeological prospecting, *Archaeological Prospecting*, Vol.2, 85-89, 1995.
- Nuzzo, L., and T. Quarta, Improvement in GPR coherent noise attenuation using t-p and wavelet transforms, *Geophysics*, Vol.69 (3), 789-802, 2004.
- Sacchi, M.D., D.J. Verschuur, and P.M. Zwartjes, Data Reconstruction by Generalized Deconvolution, in 74th Annual International Meeting, Society of Exploration Geophysicists, Expanded Abstracts, SEG, Denver, 2004.
- Theune, U., C.D. Rokosh, M.D. Sacchi, and D.R. Schmitt, Mapping fractures with GPR: a case study from Turtle Mountain, submitted to *Geophysics*, 2005.
- Ulrych, T.J., M.D. Sacchi, and J.M. Graul, Signal and noise separation: Art and science, *Geophysics*, Vol.64, 1648-1672, 1999.
- Zeng, X., and G.A. McMechan, GPR characterization of buried tanks and pipes, *Geophysics*, Vol.62, 797-806, 1997.

Dip-dependent GPR image decomposition

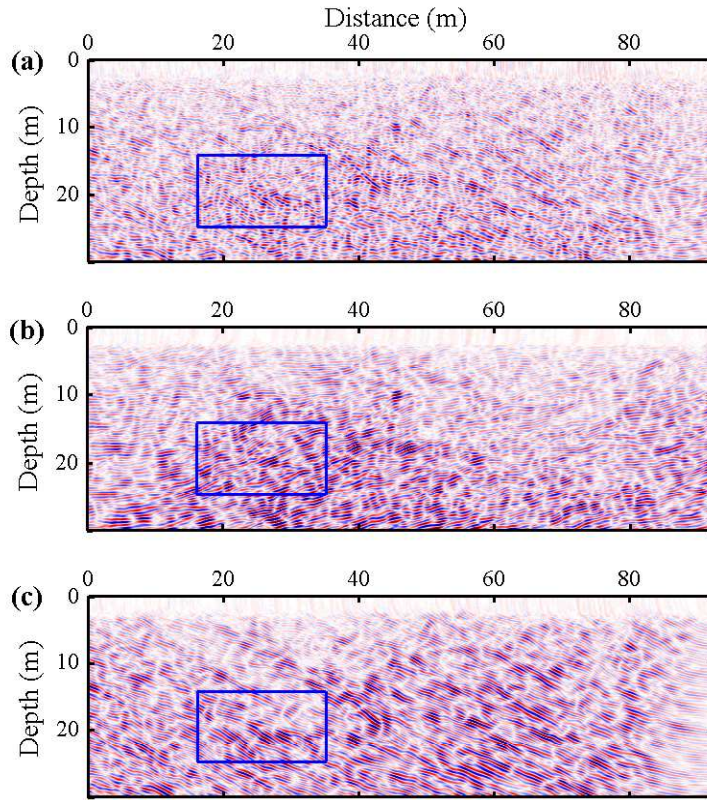


Fig. 3: Top: Detail of the migration using the original data set. Bottom left: "Upward" dipping image component, bottom right: "downward" dipping components.

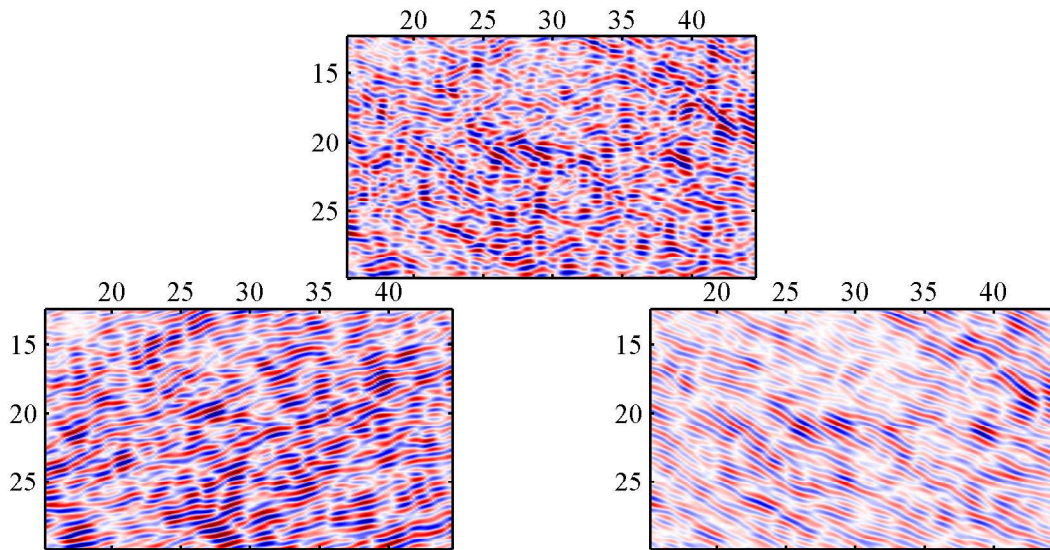


Fig. 4: a): Detail of the migration using the original data set (Fig. 3a), b): "Upward" dipping image component (detail of Fig 3b); c): "downward" dipping components (taken from Fig. 3c).